The International Journal of Advanced Manufacturing Technology (2020) 106:1223–1238
https://doi.org/10.1007/s00170-019-04371-0

ORIGINAL ARTICLE

Review and analysis of heat source models for additive manufacturing

Mohamed I. Al Hamahmy[1] · Ibrahim Deiab[2]

Received: 3 July 2019 / Accepted: 28 August 2019 / Published online: 6 December 2019

Abstract

As additive manufacturing (AM) becomes a viable manufacturing solution, demand for an accurate thermo-structural model of the process increases. Iteratively correcting discrepancies between the CAD model and additively manufactured product through trial and error can be an expensive and time-consuming process, taking up to several hours to build and costing up to tens of thousands of dollars Lindgren et al. (Addit Manuf 12:144–158, 2016). A numerical model reduces manufacturing cost and time considerably by predicting discrepancies that will arise due to the complex thermal history induced by the AM process, thus reducing the need for iterative manufacturing. An important part of any additive manufacturing model is the heat source model. The heat source model is a mathematical function which represents how much of a heat source's power actually goes into heating the powdered metal and how this heat is distributed across the heat-affected zone (HAZ). This paper provides a review and analysis of heat source models in the AM literature to date in order to alleviate some of the confusion and provide emerging researchers in the field with perspective on the issue. Both two-dimensional surface models and three dimensional volumetric models are explored. Next, an analysis of the models was performed and presented in an effort to validate their physical accuracy and mathematical usability. This analysis consisted of checking for sensible boundary conditions and ensuring that energy conservation is upheld. In surface models, the TEM_{00} model is a classic representation of the Gaussian power distribution of most heat sources used in AM. Researchers interested in simply modeling the heat distribution, without accounting for any other phenomena that intervene in the heat transfer process (such as molten pool dynamics) will find the TEM_{00} model suitable. The literature also shows cases where the TEM_{00} model has been modified to have a sharper radial gradient, and these modifications can be suitable for high-powered heat sources. For volumetric models, Goldak's ellipsoidal model (Metall Trans B 15(2)299–305, 1984) remains a straightforward and accurate model that is physically sound and applicable to a variety of cases. The Gaussian cone model presented by Rogeon et al. [48] also performs well, meeting all the required physical and mathematical restrictions. This model's linearly decaying penetration is better suited for high-energy applications. The non-Gaussian cone proposed by Tsirkas et al. (J Mater Process Technol 134(1):59–69, 2003) imposes inaccurate boundary conditions and violates the first law of thermodynamics, and is thus deemed an inadequate model. Other novel models have been introduced in recent years, most notably the line model and the elongated ellipsoidal model presented by Irwin and Michaleris (J Manuf Sci Eng 138(11):111004, 2016). Both of these models are based on Goldak's ellipsoidal model and attempt to maintain the accuracy of that model while allowing for fewer time steps and requiring less computational resources. These models appear to function well and can be used effectively in some applications, but could benefit from further study and validation. Care must be taken to ensure that the parameters used with these models do not result in averaging errors or a discontinuous thermal field. These tools must be used carefully with a thorough understanding of the underlying mathematics.

Keywords Additive manufacturing, 3D printing, Finite element analysis, FEA, Powder deposition, Powder bed, Gaussian heat source

✉ Mohamed I. Al Hamahmy
malhamah@uoguelph.ca

Ibrahim Deiab
ideiab@uoguelph.ca

[1] Advanced Manufacturing Lab, University of Guelph, 3414 Thornborough Building, Guelph, Canada

[2] Advanced Manufacturing Lab, University of Guelph, 2519 Thornborough Building, Guelph, Canada

1 Introduction

Over the last few decades, additive manufacturing (AM) has grown from a niche technology to a viable manufacturing option. Several industrial applications lend themselves to the unique benefits that AM brings, and industries such as the airline, healthcare, and automotive industries have integrated AM into their day-to-day operations alongside more conventional manufacturing methods. However, AM remains a young technology held back by an incomplete understanding of the process.

This is particularly true of mathematical modeling of the AM process, which is essential to reduce the need for expensive and time-consuming iterative builds. The numerous physical phenomena involved in the process, spanning a wide range of spatial and temporal dimensions, have challenged the collective understanding and resources of the scientific community. As the scientific literature struggles to keep up with this emerging technology and researchers around the world develop their own unique tools to address these challenges, it is important to periodically compare and scrutinize these different approaches.

An important part of any AM modeling effort is the heat source model. The heat source model is a mathematical function which represents how much of a heat source's power actually goes into heating the powdered metal and how this heat is distributed across the heat-affected zone (HAZ). The heat source model can also provide an estimation of how the powder deposition process influences the heat source and inform the design of the powder nozzle [1], as well as the complicated interactions between the molten pool and the laser spot. Issues such as varying radiative properties of the build surface due to phase change, laser attenuation by the falling powder, and penetration of the heat source into the thickness of the build are just some of the physical phenomena that a heat source model can be used to estimate in a macro-scale model of the overall manufacturing process, using empirical data.

Due to the complexity of the AM process, however, it can be difficult to establish whether or not a heat source model is functioning well. An AM model often contains several empirical constants that are established experimentally, and these constants can easily mask underlying issues with a model by providing "false" positive results—i.e., results that agree with experimental data although the theory behind them is flawed. For example, a model that overestimates laser heat transfer can be coaxed into providing valid results if it is used with an underestimated efficiency value. Since laser efficiency is empirically determined, problems can go unnoticed and later distort predictive efforts. For this reason, heat source models must be inspected in isolation to ensure that they function correctly before they are incorporated into an AM model. This paper provides a critical review of heat source models in the AM literature to date in order to alleviate some of the confusion and provide emerging researchers in the field with perspective on the issue.

2 Heat source models

Heat source models for additive manufacturing are most often derived from welding literature [2]. The interaction between the heat source and the work surface is identical in both manufacturing processes, and although AM consists of multiple-layered builds, leading to a more complicated thermal history, the surface interaction with the heat source remains the same. Below is a list of heat source models that have been used in the AM modeling literature to date.

2.1 Two-dimensional models

Some studies opt to use a two-dimensional, surface heat source model, where the heat is distributed along the deposition surface with no heat penetration accounted for. Laser penetration in this context is an analogy for multiple phenomena that occur nearly simultaneously at the transient molten region. These phenomena include increased absorptivity of metal as it melts and convection in the molten pool through the Marangoni effect.

The use of surface heat source models for modeling welding processes has been justified by numerous sources in the literature [3]. These equations have also been used extensively in additive manufacturing models. However, models that utilize these surface distributions also usually account for other forms of thermal transience independently, since the heat source model itself neglects to account for anything other than straightforward heat input from a heat source.

This section presents the surface heat source models found in the additive manufacturing literature to date.

2.1.1 TEM_{00} Gaussian distribution

In 2003, Hu and Kovacevic published a study [4] that investigated the thermal behavior of the molten pool during the laser-based additive manufacturing of a single-bead wall. Closed-loop control of process parameters was employed to maintain a constant molten pool geometry and cooling rate throughout the process. In this study, the heat source model was expressed as thermal flux density (energy per area) and was given by the formula:

$$q = 2AP\,\mathrm{e}^{\frac{-2r^2}{r_b^2}} \tag{1}$$

where A is the absorptance of the powder (dimensionless), P is laser power (W), r_b is the radius of the laser spot (m), and r is the radial coordinate at which laser intensity is being evaluated (m). The authors attribute this model to the work done by Cline and Anthony in 1977 [5]. This model is the ubiquitous TEM_{00} model, so-called because it represents the fundamental transverse mode of laser waves [6]. This fundamental mode dominates laser heat transfer when a laser is focused in a single spot, as is the case in additive manufacturing applications. This model is very common in additive manufacturing literature, as well as the literature for similar technologies.

In 2004, Han et al. [7] used this same heat source model in their model of a cladding process. Their model also accounted for the attenuation of laser power caused by the beam's interaction with the powder before arriving at the melt pool. This attenuation, for a coaxial nozzle, is adapted from the work of Frenk et al. which dealt with a side nozzle [8]. The attenuation of laser power for a coaxial nozzle is thus given by:

$$P_{atten} = P_{laser}\left[1-\exp\left(-\frac{3Q_{\text{ext}}\dot{m}l}{\pi \text{r} D_p^2 \rho V_p}\right)\right] \tag{2}$$

where $\dot{m}$ denotes the mass flow rate (kg/s), l is the flight distance from the nozzle exit to the substrate (m), D_p^2 is the area diameter covered by the powder cloud (m^2), V_p is the powder injection velocity (m/s), r is the radius of the powder particle (m), ρ is powder density (kg/m^3), and Q_{ext} is the extinction coefficient (dimensionless). This work assumed that the extinction cross section is close to the actual geometrical cross section, thus setting $Q_{ext} = 1$. Rearranging terms and expressing intensity as the power per unit area (W/m^2), we arrive at a formula for laser intensity absorbed by the workpiece after attenuated power is accounted for:

$$\begin{aligned} q_{absorbed} &= P_{total} - P_{atten} = 2AP\, e^{\frac{-2r^2}{r_b^2}} - P_{atten} \\ &= 2AP\, e^{\frac{-2r^2}{r_b^2}} - P\left[1-\exp\left(-\frac{3\dot{m}l}{\pi r D_p^2 \rho V_p}\right)\right] \\ &= \mathrm{P}\left[2A\, e^{\frac{-2r^2}{r_b^2}} + e^{\left(-\frac{3\dot{m}l}{\pi r D_p^2 \rho V_p}\right)} - 1\right] \end{aligned} \tag{3}$$

Qi et al. [9] presented another model of the direct deposition process in 2006 using the same TEM_{00} equation for laser intensity distribution. Citing the Beer-Lambert law, the authors also present a different formulation for the attenuation of the laser beam through coaxial powder flow. This formulation is given by

$$q(r,l) = q_l(r)e^{(-\sigma_{ext}Nl)} \tag{4}$$

where σ_{ext} is the mean extinction area of powder particles (m^2) and N is the number of powder particles in a given control volume.

Additionally, the temperature increase in the powder during the deposition process is given by

$$q(r,l)\alpha\pi r_p^2\left(\frac{\Delta l}{v_p}\right) = \frac{4}{3}\pi r_P^3 \rho_p C_p^p \Delta T \tag{5}$$

which describes the energy balance between the portion of attenuated power that is absorbed by the powder and the powder's thermal capacity.

Roberts et al. [10] presented a study in 2009 that examined the transient thermal field during laser melting of metal powders in additive manufacturing. This study is particularly relevant to this current review as it was concerned singularly with the thermal aspects of the process. This study uses the same heat source model described above to represent the distribution of laser heat across the surface of the laser spot and correctly identifies it as the fundamental transverse mode of laser irradiance, TEM_{00} [11]. This thermal model was then validated using the experimental findings of Fischer et al. [12]. Following this study, Lavery et al. [13] presented a conference paper in 2014 that included a brief review of additive manufacturing modeling efforts to date. In addition, the paper explored several modeling case studies, one of which looked at the effect of thermal-structural coupling on simulation results for the simple case of a moving heat source on a rectangular plate. Results indicated a notable difference in residual stress calculation when thermal and structural modeling components are uncoupled (the structural problem is solved following the thermal problem with no iteration between the two). However, further investigation and validation are required. This heat source model is also cited as the most widely adopted model in the literature by Zeng et al. [14] in their comprehensive review of laser sintering and selective laser melting. There is a slight misspelling in their paper where the number "2" is missing from the exponential numerator in their Eq. 5, but the model is clearly intended to be the very same TEM_{00} model.

Several other studies have utilized this two-dimensional TEM_{00} Gaussian distribution. Alimardani et al. [15] used this model in their study where they carried out a numerical and experimental investigation on the thermal history and stress field induced during the formation of a thin-wall part using laser solid freeform fabrication, an additive manufacturing process that involves movement of the substrate. The incidence angle of the laser was also taken into account whenever the deposition surface was not flat by modifying the absorption factor [16, 17]. Kovalev et al. [18] utilized this formulation in their study of gas-dispersed powder deposition in a Direct Laser Deposition (DLD) AM process, citing Toyserkani et al.'s textbook on laser cladding [19]. They compared three different coaxial designs and performed a multiphase computational analysis, developing an algorithm to model the particle follow pattern based on material properties and

nozzle geometry. Foteinopoulos et al. [20] used this formulation in their 2D model of the selective laser sintering (SLS) additive manufacturing process. They aimed to build a model that was both computationally efficient and accurate. An adaptive meshing strategy was used to reduce computational time and enable storage of the entire thermal history of the process. Material properties were not only temperature-dependent, but also porosity dependent, using relations developed by Maxwell [21] and German and Park [22].

An alternative formulation of the 2D Gaussian distribution was used by Manvatkar et al. in several of their studies on LENS and DLD processes [23–25]. The first study presented a thermal model of a single-layer LENS process that predicts parameters such as layer height, cooling rate, and molten pool temperature and dimensions. The second and third studies further developed this model for multilayer DLD processes, additionally accounting for laser attenuation and powder heating mid-flight through coaxial deposition. The heat source model used in all three studies is given by:

$$q = \eta P d \exp\left(-\frac{d r^2}{r_{eff}^2}\right) \tag{6}$$

where d is known as the laser energy distribution factor. This formulation is used more frequently in the welding literature, although the selection of laser power distribution factor appears empirical. It can be set to 2 to obtain the conventional 2D TEM_{00} model that has been discussed so far. In these three studies, however, this distribution factor was set to three, representing a steeper distribution with more intensity at the center of the spot and a sharper decline in intensity radially outwards. In the first study, the authors state that this steeper distribution is better suited to the type of laser used in the LENS process, which was a diode pumped ytterbium fiber laser used at a 210-W laser power. The latter two studies do not state the type of laser used, but due to the similarity in process parameters between the first study and the second, it can be inferred that the same laser was used for both studies. Mukherjee et al. [26] subsequently used this same formulation in their coupled thermal-structural model, which also involved modeling of fluid flow in the molten pool. All four studies that used this formulation were experimentally validated.

Huang et al. [27] carried out a study in 2004 that focused on the attenuation of the laser beam through the powder deposition, and reached several formulations that express the attenuated laser power. In this study, the laser energy distribution factor described above is taken as 1, resulting in the following formulation:

$$q = P \exp\left(-\frac{x^2 + y^2}{R_1^2}\right) \tag{7}$$

The choice of a distribution factor of 1 is not addressed in the study; it may have been used to represent a lower power heat source using a gentler distribution slope representing a more even distribution. Next, the authors used the Beer-Lambert theorem [28], which gives the attenuation of the laser when traveling through a medium using the equation

$$q(x,y,z) = q(x,y,z+\Delta z)\left\{1 - \exp\left[-\pi R_p^2 . N(x,y,z) . k(\Delta z)\right]\right\} \tag{8}$$

where $q(x, y, z + \Delta z)$ is the incident laser intensity before attenuation (W/m^2), and R_p is the mean radius of powder particles (m). $N(x, y, z)$ is the particle concentration in the path of the beam, and $k(\Delta z)$ is known as the extinction coefficient or attenuation coefficient and is dependent on the laser's wavelength and powder properties. This attenuation coefficient is given by Mie's solution to the Maxwell equations [29] as

$$k = \frac{\lambda}{\pi R_p} \sum_{n=0}^{\infty} (2n+1)\left(|a_n|^2 + |b_n|^2\right) \tag{9}$$

where λ is the laser wavelength, and $a_n$and $b_n$are known as the Mie coefficients, which are given by Riccati-Bessel functions and spherical Bessel functions. These functions are usually solved using recursive algorithms [30, 31] in a mathematically involved process. Additionally, the heat absorbed by powder particles as they are deposited is calculated independently, utilizing the key assumption that the temperature gradient among the particles does not vary radially. As such, the laser power absorbed by the powder particles during deposition is calculated in a layer-by-layer fashion (relative to vertical height from the substrate) and is given by

$$Q = I(x,y,z).\alpha_P - 2\sigma\epsilon\left(T^4 - T_{surroundings}^4\right) - h_f\left(T - T_f\right) \tag{10}$$

which is simply representative of the energy balance between the absorbed laser power (α_P being particle absorptivity) and heat loss to the surroundings through radiation and convection.

2.1.2 Combination of TEM00 and TEM01

While the fundamental mode TEM_{00} yields sufficiently accurate results for most studies, Kovalev et al. [32] employed a more sophisticated application of optical modes in their study of the DLD process. Their model was focused on the prediction of molten pool geometry and size, starting with the powder delivery gas flow field, particle dispersion, and all the way to the interaction with the substrate. Convection within the molten pool due to the Marangoni effect was neglected. Following the technical specifications of the Trumpf DMD505 facility,

where the validating experiments were conducted [33–35], the heat source model used was a linear combination of the radiation modes TEM_{00} and TEM_{01}:

$$q = 2P\left(a_{00} + a_{01}\frac{2r^2}{r(z)^2}\right)\exp\left(-\frac{2r^2}{r(z)^2}\right) \tag{11}$$

where

$$r(z)^2 = r_0^2 + (z-z_0)^2\left(\frac{D_f}{2F_d}\right)^2 \tag{12}$$

The coefficients a_{00} and a_{01} determine the ratio of TEM_{00} and TEM_{01} in the linear combination and are determined experimentally (values of 0.25 and 0.75, respectively, are used in this study). z_0 is the vertical position of the focal plane, D_f is the lens diameter, and F_d is the focal distance. This formulation thus takes into account the location of the laser spot relative to the beam waist as opposed to assuming that the laser is always operating at the waist. This is an important factor to consider especially in the DMD process, where layers are built on top of one another with no movement in the substrate. On the other hand, the assumption that the beam is always operating at the waist is safe to make when it comes to SLS processes, since the substrate moves downward with every deposited layer, maintaining a constant distance between the laser and the molten pool.

2.1.3 Circular distribution

An alternative two dimensional heat source model is the circular distribution, used by Peyre et al. in their thermal DMD analytical-numerical model [36]. The circular heat source model is given by the following equation:

$$q = q_0 \cdot \sqrt{1-\left(\frac{x^2}{r_0^2}\right)-\left(\frac{y^2}{r_0^2}\right)} \tag{13}$$

This study briefly explored the difference between Gaussian and circular heat distributions and found that the circular distribution is valid for the 5–7 mm defocusing range. Powder absorptance is accounted for when calculating laser power attenuation, which follows the work of Qi et al. discussed above. The thermal results obtained using this model were validated experimentally.

Citing Peyre et al.'s comparison between Gaussian and circular distributions, Zhao et al. [37] also chose to use a circular distribution in their thermal and structural model of SLS additive manufacturing of titanium alloy parts. This study investigated aspects of molten pool size, cooling/heating rates and residual stresses using a coupled modeling methodology. A three-dimensional model was used to explore these parameters in a single-layer build, and a two-dimensional model explored multiple layer builds. Experimental validation was not performed and is stated to as a future area of work.

2.2 Three-dimensional models

Following the discussion of surface heat source models, this next section presents a discussion of volumetric heat source models found in the additive manufacturing literature. These heat source models are characterized by a three-dimensional profile that attempts to approximate transient heat transfer mechanisms at the molten pool, accounting for phenomena such as the change in absorptance of the powder as it changes phase and convection effects within the pool. These models all involve parameters that must be determined empirically, such as laser penetration depth. Many varied three-dimensional geometries are used by different researchers to model heat distribution, whereas the two-dimensional models all involve radial exponential decay of heat (with only the gradient of that decay varying from model to model).

2.2.1 Gaussian ellipsoid model

This model consists of Gaussian functions in all three dimensions, leading to a half-ellipsoidal geometry. It dates back to 1984, when Goldak et al. published their seminal formulation of a double-ellipsoidal model for finite element analysis of welding heat sources [38]. First, they justify the use of a Gaussian surface distribution of the heat source, stating that models that assume a constant power density in the molten zone, such as the model developed by Paley and Hibbert [39], are both physically inaccurate and mathematically undesirable. They are physically unrealistic because they does not satisfy stirring velocity boundary conditions, which must be zero at the fusion zone boundary and maximum at the heat source-metal interface, and they are mathematically undesirable since they lead to a large thermal impulse at the edge of the spot size, which requires excessively large mesh densities in order to be computed adequately. The ellipsoidal Gaussian distribution is presented as a preferable alternative that is in strong agreement with experimental measurements. The use of a volumetric distribution is justified by the need to account for heat penetration beneath the surface of the material as well as molten pool complexities that are difficult, if not impossible, to model, such as the effects of surface tension and buoyancy forces.

The double-ellipsoidal heat input model is formulated by defining an ellipsoidal three-dimensional Gaussian distribution, applying conservation of energy constraints, and defining boundary conditions at the edge of the ellipsoid. The boundary condition used by Goldak et al. is that the heat intensity at the edges of the ellipsoid (i.e., the edges of the heat source spot) in any of the

three axes is equal to 5% of the maximum intensity. These conditions lead to the popular formulation:

$$q(x,y,\xi) = \frac{6\sqrt{3}Q}{abc\pi\sqrt{\pi}} e^{-3x^2/a^2} e^{-3y^2/b^2} e^{-3\xi^2/c^2} \quad (14)$$

where ξ is a longitudinal coordinate on an axis whose origin remains stationary as the heat source travels across the workpiece and is defined by:

$$\xi = z + v(\tau - t) \quad (15)$$

where v is the travel speed of the heat source and τ is a lag term used to define the location of the heat source at $t = 0$. This double-ellipsoidal geometry is more flexible than other alternatives and allows the formulation to account for a variety of heat sources, including non-axisymmetric ones. This model was validated against Christensen's [40] and Chong's [41] experimental investigations, as well as the numerical investigation conducted by Krutz and Segerlind [42], who used the surface disk model presented by Pavelic et al. [43]. The model was validated successfully, showing strong agreement with these experimental results and demonstrating a more accurate temperature distribution around the weld than the surface disk model presented by Pavelic et al.

This formulation is the most commonly used in AM models. Michaleris [44] used this formulation in his 2014 study where he investigated the different ways with which to model material addition in a finite element model. The first method he studied was the quiet element method, where the entire geometry of the part is created at the beginning of the simulation, but material that will be added later in the process is turned "quiet" by temporarily reducing its thermal conductivity and specific heat capacity to near zero. This ensures that the material will have no thermodynamic effect on the model until it is physically relevant, i.e., it has been added to the model. At that time, its original material properties are restored. This method has the advantage of having one constant matrix formulation throughout the entire modeling process, with no need to re-generate the matrix equation after every deposition step. On the other hand, this model must solve the same number of equations whether the process has just started or is nearly done, meaning that this method does not make use of the initial small number of active elements for faster computation times. The second method investigated in this study is the inactive element method, where elements representing material that will be deposited later in the process are removed from the analysis entirely until the process arrives at the stage at which this material is added. Because the number of elements in the model is therefore much smaller at the start of the process, this model benefits from faster computational times specifically at the initial stages of the deposition process. However, this method cannot be easily incorporated into most commercial FEA software, and the faster computation time may be offset by the need to reformulate the problem at every time step. Using a case study of a thin wall build on top of a substrate, Michaleris found that the difference in computational time between both methods is insignificant if the method is applied adequately.

Similarly, Heigel et al. [45] also investigated the relevance of accurate forced convection values in the overall accuracy of a finite element model of the DLD process. Three different DLD processes were considered, using Ti-6Al-4V as the work material. Three thin-walled geometries were considered with a different idle time for each geometry. Each of these three test cases was run twice: once using in situ measurements of forced convection, and once with only free convection considered on all surfaces. The results of the model were compared with experimental results and verified that neglecting to include forced convection in the model accounted for an increase in percentage error of up to four times.

Yang et al. [46] also used Goldak's Gaussian ellipsoid model in their thermomechanical model of the LENS process. Their model, published in 2016, utilized both a quasi-static and a full transient coupling of the thermal and structural analyses. The quiet element method was used to simulate metal deposition. The LENS process being modeled consisted of five layers of a square contour being built on top of the substrate. The model was validated through experimentation, finding good agreement between experimental and numerical results. The increase in accuracy when using full transient coupling between the thermal and structural models as opposed to quasi-static coupling was determined not to be worth the severe increase in computational cost.

Denlinger and Michaleris developed a finite element model of the DLD process in 2016 [47] in order to study the effect of stress relaxation on the residual stress experienced by the part during manufacturing. The study developed a method to numerically account for the effect of transformation strain, which sometimes acts in opposition to all other strain components and thus helps mitigate residual stresses during AM. The effect was studied in Ti-6Al-4V and compared to the behavior of Inconel 625, since the latter does not experience any allotropic phase changes and thus serves as an adequate benchmark. A DLD process was simulated using varying idle times between each pass; since decreasing idle time increases the molten pool temperature for subsequent passes, the effect of transformation strain is more pronounced at shorter idle times. The study confirmed that shorter idle times, leading to increased transformation strain, reduced residual stresses when machining Ti-6Al-4V, leading to less distortion. The opposite was observed when Inconel 625 was used; since Inconel 625 does not undergo allotropic phase change, there was an absence of transformation strain to counteract the thermal stresses that became more severe as the idle time was decreased. Therefore, Inconel 625 experienced more severe distortion and residual stresses as idle time was reduced. The numerical findings of this study were validated experimentally, and provide compelling evidence that any optimization strategy for

the DLD process will be inadequate if allotropic phase change is not taken into account.

2.2.2 Conical models

The Gaussian cone heat source model is a more recent formulation. Geometrically, it can be described as a two-dimensional Gaussian distribution in the *x*-*y* plane that decays linearly in the *z*-axis (i.e., the penetration axis). It is therefore this linear decay along the penetration axis, as opposed to a Gaussian decay, that sets this model apart from Goldak's ellipsoidal model. This model geometry is represented by several different formulations in the literature. The most prominent are presented below.

a. Gaussian Cone:

A formulation of the conical Gaussian heat source was given by Rogeon et al. [48] in 2001. This formulation was developed through several experiments for electron beam welding, and was then formally expressed by Rouqette [49] as:

$$q(x,y) = f(z_e) * \frac{8\eta UI}{\pi \emptyset_E^2} \exp\left(- \frac{8\left(x^2 + (y - y_s)^2\right)}{\emptyset_E^2} \right) \tag{16}$$

where $f(z_e)$is given by the equation:

$$f(z_e) = \frac{2}{h}\left(1 - \frac{z_e}{h}\right) \tag{17}$$

Using a notation more consistent with previous formulations, we can rewrite the previous two equations as:

$$q(x,y,z) = \frac{16\eta Q}{\pi r_0^2 h} \exp\left(-8\frac{r^2}{r_0^2}\right) * \left(1 - \frac{z_e}{h}\right) \tag{18}$$

This formulation was used in an AM context by Shen and Chou [50] in 2012, who used this heat source formulation in their thermal model of an electron beam additive manufacturing (EBAM) process. This thermal model was validated against experimental data found in the literature and then used to explore the effect of porosity-dependent powder properties and beam diameter on the EBAM process. This study found that an increase in powder porosity caused an increase the molten pool temperature along the *z*-axis, but resulted in a decreased temperature in the *x*-*y* plane. The overall molten pool temperature was seen to increase with higher porosity powders. Heating and cooling rates of the metal powder were seen to decrease with increasing porosity. These results indicate that powder porosity is likely an optimizable parameter, where increased porosity can decrease cooling rates during solidification leading to a more homogeneous product, but decreased porosity leads to more dense parts with a smaller likelihood of trapped air bubbles interfering with part quality.

This formulation was also used by Romano et al. [51, 52] in their thermal finite element model of the laser AM process. This study investigated the molten pool size and temperature for three different materials in order to find the difference in process parameters needed to successfully additively manufacture parts using each material. The model was fed with the material properties of stainless steel (SS316L), Aluminum (Al7075), and Ti-6Al-4V. The study indicated that Aluminum required the highest heat input in order to maintain an adequate melt pool for manufacturing, even though it possesses the lowest melting point of the three metals. This is attributed to aluminum powder's low absorptivity and solid aluminum's high conductivity. These attributes mean that the powder is not absorbing as much of the lasers heat as alternative metals and dissipates it to the surrounding area through conduction at a higher rate, making it difficult to maintain an adequate molten pool. Titanium was found to require the least heat input out of the three metals.

b. Non-Gaussian cone:

This first Gaussian cone formulation first appeared in 2002, when Tsirkas et al. [53] presented a finite element model of laser welding in order to predict distortion caused by the welding process. This model used a cone geometry to represent the keyhole-shaped heat distribution that has been widely recorded in the literature for high-powered laser applications. The cone distribution of power density is given by the following equation:

$$q(r,z) = \frac{2Q}{\pi r_0^2 H} e^{1 - \left(\frac{r}{r_0}\right)^2} \left(1 - \frac{z}{H}\right) \tag{19}$$

where Q is the laser power absorbed by the work piece each time step, r_0 is the spot radius, H is the depth of penetration of the laser, and (r, z) are the radial coordinates of each node at which the power density is being calculated, with the origin being the center of the laser spot.

This formulation was later used by Wang and Felicelli [54] in developing a model to investigate the influence of LENS processing parameters on phase transformations and discussed the implications on part hardness. The study discovered that sufficiently fast laser travel speeds are needed to reduce the occurrence of tempered martensite, resulting in a more uniform microstructure and hardness of the product. However, faster laser travel speeds can result in incomplete fusion of the metal powder particularly in the lower layers nearer to the substrate, which results in porosity of the product. Therefore, sufficiently high laser power must be used in conjunction with faster laser travel speeds to produce a homogenous, suitably dense product. Wang et al. [55] then

further developed this model of the LENS process for the purpose of investigating the relationship between laser power and molten pool size for multiple layer builds. First, the model was validated against experimental results presented by Hofmeister et al. [56]. The model was then used to investigate the relationship between laser power and molten pool size and found that for the parameters they were investigating, a constant molten pool size resulted in a near-linear decrease in laser power for increasing layer numbers, when accounting for initial transience caused by the cold substrate. The model also verified the necessity of increasing laser power when travel speed is increased in order to maintain a constant molten pool size. Finally, in a third study, Wang et al. [46] further developed the model to investigate the effect of LENS process parameters on residual stresses experienced by the part during manufacturing. These numerical results were then validated using experimental neutron diffraction stress measurements, although the authors maintain that further validation is necessary for a wider range of values to ensure the predictive ability of the model. Within the scope of the investigated parameters and values, the study indicates that higher laser power increases residual stresses, as expected. The correlation with laser travel speed is more complex and was not entirely clear; certain speeds caused compressive residual stresses along the height of the piece (perpendicular to layer deposition) while other speeds caused tensile residual stresses. Further study is needed to explore this relationship. This formulation was also used by Piekarska and Kubiak [57] who presented their own thermal model of laser welding S450 steel sheets in 2012.

2.3 Other three-dimensional models

The following models have only been proposed by a single study each. They may offer some merit but require further investigation.

2.3.1 Line and elongated ellipsoid models

Irwin and Michaleris [58] published a study in 2016 presenting new heat source models for powder bed additive manufacturing. The models were created to address the issue of exceedingly small time steps needed to accurately represent the small spot sizes that characterize powder bed AM, allowing it to achieve high-resolution builds. A formulation that allows the use of larger time steps can benefit from considerably shorter computation times.

This study offers two alternatives to the classic Gaussian ellipsoid model formulated by Goldak. The first is the line model, which essentially averages the heat input given by Goldak's ellipsoidal model over the length of several time steps, allowing the computation of up to an entire pass of the laser in a single time step. This line model is given by the following integral:

$$Q = \frac{1}{\Delta t}\int_{t_0}^{t_0+\Delta t} Q\,dt$$
$$\therefore \bar{q} = \frac{3P\eta}{\Delta t v_s ab\pi}\exp\left(-\frac{3x^2}{a^2}-\frac{3y^2}{b^2}\right)\mathrm{erf}\left(\frac{\sqrt{3}(z+v_s t)}{c}\right) \tag{20}$$

The line model allows the time step to be increased without fear of skipping over elements, which is a concern with Goldak's ellipsoidal model. However, if a time step is used that results in a much greater line segment (along the deposition direction) than the diameter of the spot size, the line model results in near-discrete steps of thermal energy. This sort of discontinuity is physically invalid and will produce inaccurate results if left unmitigated.

To address these discontinuities, an elongated ellipsoidal model is proposed. This model operates by adjusting the intensity at the edges of the ellipsoid to be equal to half the maximum intensity, which occurs at the center of the ellipsoid. This then allows the ellipsoid to be "stretched out" over a larger portion of the pass length. An adjusted pass length must be used, which is given by the equation:

$$\tilde{c} = \frac{v_s \Delta t}{2}\sqrt{\frac{3}{\log 2}} \tag{21}$$

This elongated ellipsoid can now be expressed as:

$$q(x,y,\xi) = \frac{6\sqrt{3}Q}{ab\tilde{c}\pi\sqrt{\pi}}\exp\left(-\frac{3x^2}{a^2}-\frac{3y^2}{b^2}-\frac{3\left(z+v_s\left(t_0+\frac{1}{2}\Delta t\right)\right)^2}{\tilde{c}^2}\right) \tag{22}$$

The authors then proceeded to test both of these models in comparison to Goldak's model, using a process that involves five uni-directional heating passes on top of a rectangular substrate. Multiple time steps were used with each of the proposed novel models to demonstrate their behavior with varying time steps. The study found that accurate results (within 10% of Goldak's model) can be obtained using these formulations. The line model was found to produce more accurate deformation results, while the elongated ellipsoid model performed better during thermal analysis.

2.3.2 Three-dimensional TEM00 model

A three-dimensional TEM_{00} model was used by Vasquez et al. in 2011 [59]. Their model of the DLD process was aimed primarily at predicting the shape and size of the molten pool. The thermal model took into consideration convection due to the Marangoni effect, as well as laser power attenuation due to powder delivery as described by Han et al. [7] earlier. The heat source model in this study is given by:

$$q = \frac{2}{\pi r^2} P e^{\frac{-2}{r^2}\sqrt{x^2+y^2+z^2}} \tag{23}$$

The transverse modes of radiation are, by definition, two-dimensional; they describe the variation in radiation intensity in a plane that is perpendicular, or "transverse," to the direction of irradiance. The physical reasoning behind this three-dimensional formulation of the TEM_{00} equation is therefore unclear.

The study was validated using the experimental work of Lalas et al. [60], and a strong agreement between the predicted and actual molten pool geometries was observed. The study then proceeded to investigate the expected effect of various process parameters on molten pool geometry. An increase in powder flow rate or laser scan speed was found to reduce the depth of the molten pool. An interesting relation was found between metal evaporation and laser power: Past a certain threshold, an increase in laser power counterintuitively decreases the amount of metal vapor escaping the molten pool. This is hypothesized to be because of the pressure applied by plasma on the surface of the base material, which traps the vapor until the molten pool cools and the vapor solidifies. These findings were consistent with the findings of Sankaranarayanan and Kar [61].

2.3.3 Logarithmic decay model

Yu et al. [62] presented a 3D model of the SLS process in 2016 that focused on the effect of re-melting densification on porosity of the manufactured part. This multi-physics model considered the behavior of gas bubbles in the molten pool and the effect of the pool's surface tension. This study found that re-melting previously deposited layers greatly reduced product porosity, which justifies lower laser scanning speeds despite a prolonged process time. The heat source model used in this study is given by:

$$q = \frac{3c_s PA}{\pi H\left(1-\frac{1}{e^3}\right)} \exp\left[-\frac{3c_s}{log\left(\frac{H}{z}\right)}\left(x^2+y^2\right)\right] \tag{24}$$

where c_s is a constant shape coefficient that is dependent on the laser emitter geometry. This heat source model is attributed to the work by Bag et al. in developing an adaptive welding volumetric heat source [63]. In their paper, Bag et al. described a heat input model comprised of two parts: a two-dimensional Gaussian distribution is used while the substrate is below melting temperature. Once the substrate dips below the solidus point, this model is replaced by a three-dimensional heat input model that accounts for the molten substrate. It is not clear how this welding model by Bag et al. led to the above model by Yu et al. One criticism that can be offered against it is that it utilizes a logarithmic fraction with the z-coordinate as a denominator. This leads to a mathematically discontinuous function which is undesirable in a numerical process. This discontinuity will also demand increased mesh density along the z-axis in order to minimize errors, increasing computation time.

3 Discussion and analysis of heat source models

A near exhaustive list of the heat source models that have been used in the additive manufacturing literature has been presented. Although most of these models will provide reasonably accurate results if tuned correctly using experimental data, some heat source models do not obey physical boundary conditions, or contain mathematical expressions that are not conducive to a numerical solution. Even physically inconsistent heat source models will yield acceptable results if they are tuned with experimental data. The additive manufacturing process, complex as it is, requires the use of empirical data in the form of constants and efficiency factors in order to be modeled accurately. However, this use of empirical data can mask modeling errors. A model that does not accurately represent the physical process can be easily coaxed into yielding results that coincide with experimental data. For instance, one of these empirical constants is laser efficiency, which represents the percentage of laser radiation that is absorbed by the work surface. If a heat source model were to underestimate the heat transferred to the work surface, this could be compensated for by using a higher value of laser efficiency. In this regard, accurate results can be obtained for specific cases even if the heat source model is flawed.

This section presents an investigation into the validity of the heat source models discussed thus far. This is performed by investigating the boundary conditions of each source, as well as checking to ensure energy conservation principles are upheld.

3.1 Two-dimensional models

To characterize these surface models and assess their validity, conservation of energy will be examined by calculating how much of the incident laser radiation is accounted for by each model. The conservation of energy will be expressed as a ratio of Q_{Actual}, the actual total energy emitted by the laser, and Q_{Model}, the total energy emitted by the heat source that the heat source model accounts for. Additionally, the ratio of peak intensity (at the center of the laser spot) to the minimum intensity (at the edge of the laser spot) will be calculated to indicate the rate of radial decay of laser energy. This ratio is referred to in this work as the intensity boundary condition (I_{bc}). Ultimately, the intensity boundary condition must reflect the physical behavior of the heat source at hand. As discussed earlier, studies have indicated that sharper radial declines in intensity are more suited for higher powered heat sources (200 W and above), leading to a lower intensity boundary condition.

3.1.1 TEM00 Gaussian distribution

The TEM_{00} model was developed several decades ago and validated through numerous experiments and studies. There is no lack of evidence to support it; it therefore serves as a good benchmark in this current work for other models.

First, the model is tested for energy conservation. This is done by integrating the intensity relation described in Eq. (1) over its entire domain and range.

$$Q_{Model} = \int_{-b}^{b}\int_{-a}^{a} q(x,y)\,dx\,dy = \int_{-b}^{b}\int_{-a}^{a} \frac{2AQ_{Actual}}{\pi r_b^2} e^{\frac{-2(x^2+y^2)}{r_b^2}}$$

$$= \frac{2AQ_{Actual}}{\pi r_b^2}\int_{-b}^{b}\int_{-a}^{a} e^{\frac{-2(x^2+y^2)}{r_b^2}}$$

$$= \frac{2AQ_{Actual}}{\pi r_b^2}\cdot\frac{\pi r_b^2}{2}\,\mathrm{erf}^2\sqrt{2} \cong 0.911 Q_{Actual} \quad (25)$$

where the variable P has been replaced with Q_{Actual}, representing the actual heat input delivered by the laser. The theoretical heat input Q_T is the total heat input that is accounted for within the model. Therefore, the model accounts for a little over 91% of the input laser power. The 9% losses can be attributed to the need to discretize an inherently asymptotic relationship. In order to maintain computational efficiency and numerical robustness, the asymptotic Gaussian decay of a heat source must be discretized to a finite domain. When this is done, a decision must be made as to the cutoff point at which further heat input will be neglected.

The intensity boundary condition serves as an indication of the rate of heat decay over the radius of the spot. A high intensity boundary condition indicates a slow radial decline in intensity, and a low intensity boundary condition implies a sharper decline.

By doing so, the ratio is found for the TEM_{00} model to be 13.5%; that is, the heat intensity at the edge of the spot is 13.5% of the peak intensity at the center of the spot. This is the industry standard, and the most common way to define the boundaries of the Gaussian irradiance, suitable for most conventional uses.

It is important to note that the two values calculated above only indicate whether or not the heat source model is consistent with the known physical characteristics of a TEM_{00} distribution. However, a model can satisfy the energy conservation criteria, and present a physically sound intensity boundary condition, and still be in other ways inappropriate. Failing to meet energy conservation criteria indicates that the model is inadequate, but succeeding in meeting these criteria does not guarantee adequacy. There are other factors that must be taken into account, such as the trend of the decay itself and whether it matches experimental observations.

Next, consider the modified TEM_{00} model with a laser distribution factor of 3, as given by Eq. (6). Applying the same analysis to this model yields the following results:

$$Q_{Model} \cong 0.972 Q_{Actual} \quad (26)$$

as well as an intensity boundary condition of 5.0%. Increasing the laser distribution factor therefore improves both metrics, meaning the model is now more physically consistent than the "classical" TEM_{00} model. A lower intensity boundary condition also indicates more computational efficiency and ease of numerical use; a higher boundary condition causes a discontinuity in the thermal field which requires a smaller mesh and/or shorter time step to compute. Judging by these metrics, the TEM_{00} model appears to more accurately represent the energy transfer of TEM_{00} irradiance when a laser distribution factor of 3 is used. However, what these metrics do not consider is the shape of the radial decay of irradiance, since increasing the laser distribution factor shifts more of the heat load towards the outer portions of the distribution. Fig. 1 illustrates this difference. The claim that a laser distribution factor of 3 is more suited to high-power applications requires further investigation.

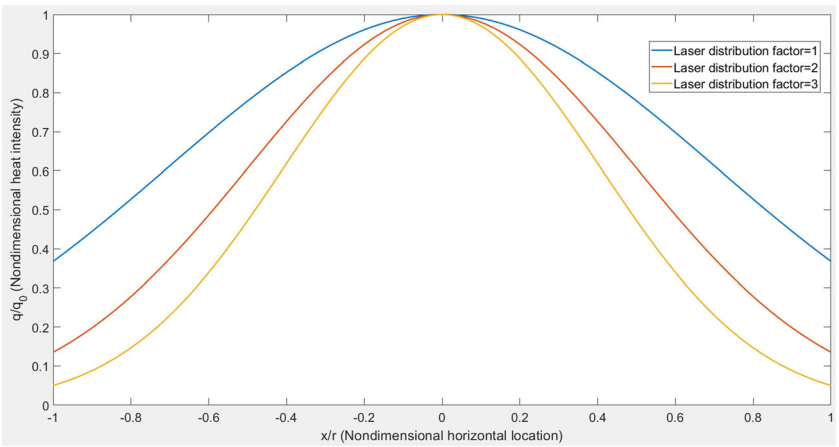

Fig. 1 TEM_{00} distribution for different laser distribution factors

Finally, repeating the analysis for a laser distribution factor of 1 as shown in Eq. (7) yields:

$$Q_{Model} \cong 0.710 Q_{Actual} \tag{27}$$

and a boundary condition of 36.79%. Using distribution factor of 1 causes considerable discontinuities in the thermal field and neglects to account for nearly 30% of the incident laser radiation, and is therefore discouraged.

3.1.2 Combination of TEM00 and TEM01

One key assumption must be made in order to apply the same analysis to the linear combination of TEM_{00} and TEM_{01} modes shown in Eq. (11). This assumption is that the deposition surface of the substrate exists at the focal plane of the laser. This equates the term $r(z)$ in Eq. (12) to r_0, the radius of the laser spot, and enables a much more transparent comparison to other heat source models. Researchers should strive to maintain the deposition plan at the focal plane of the laser in any case, as it allows for the most efficient use of the laser.

Applying this assumption, and following the procedure outlined above, the total energy accounted for by this model is given by:

$$Q_{Model} \cong 0.958 Q_{Actual} \tag{28}$$

The intensity boundary condition, on the other hand, yields a more complicated result. By evaluating the intensity at the center and dividing it by the intensity at the edge of the spot, the result is:

$$I_{bc} = \frac{q(r_0)}{q(0)} = \frac{a_{00} + 2a_{01}}{a_{00}} e^{-2} = \left[1 + \frac{2a_{01}}{a_{00}}\right] e^{-2} \tag{29}$$

indicating that the boundary condition is dependent on the ratio of TEM_{00} and TEM_{01} used in the linear combination. The larger the fraction of TEM_{01} used, the more the energy distribution is shifted towards the edges of the spot and away from the center. For the values used by Kovalev et al. [32] of 0.25 and 0.75 for a_{00} and a_{01}, respectively, the boundary condition is evaluated as 94.73%, indicating that there is hardly any decrease in intensity from the center to the edge of the spot. This highlights the limitations of using the intensity boundary condition as a measure of physical accuracy, as it is only valid for TEM_{00} models. In a pure TEM_{01} distribution, the outer edges of the laser spot are highlighted by high intensity as shown in Fig. 2. Therefore, comparing the intensity at the center of the spot to its edges does not provide a useful metric when other transverse modes are introduced. Using the intensity boundary condition as a measure of physical consistence is therefore only effective for TEM_{00} models

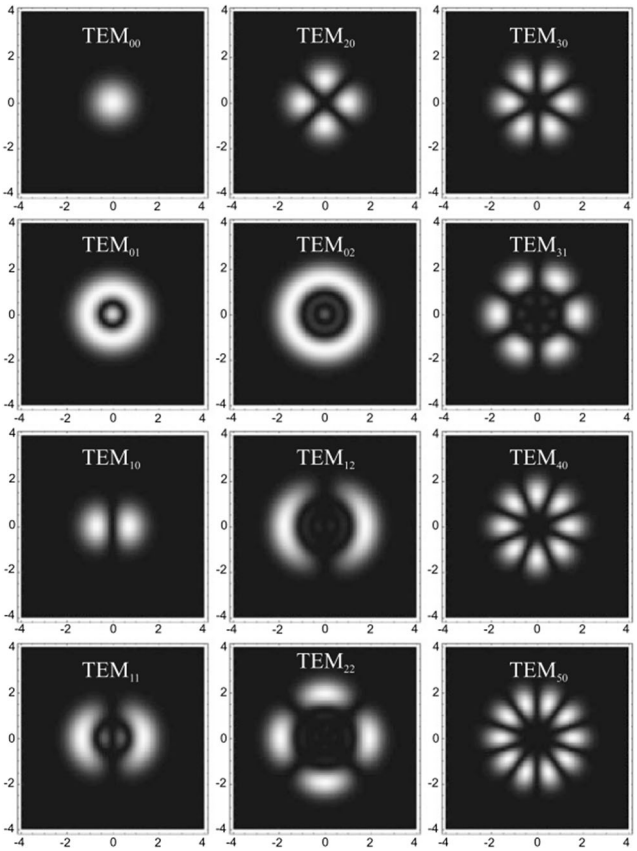

Fig. 2 Intensity distributions of some Laguerre-Gaussian beams (TEM_{ip} modes) as presented by Sargent et al. [64]

which follow a strictly Gaussian distribution. Although lasers in additive manufacturing are most commonly operated at TEM_{00} (since it provides the most efficient transfer of energy for this purpose), experimental parameters determine what transverse mode a laser will exhibit, and the heat source model used must reflect that.

3.1.3 Circular distribution

First, the circular distribution given by Eq. (13) is integrated over its domain and range to check its adherence to energy conservation principles. It was quickly found that the distribution is divergent; for any value of y such that $y \neq 0$, this model yields an imaginary number when $x = r$ (i.e., at the edge of the spot). This model is therefore not a sound representation of the intensity distribution of the laser.

It is expected that the equation presented in this study was misprinted, since Peyre et al. provided a graph of their heat source model comparing it to a Gaussian distribution, and this graph cannot be reproduced by the provided equation. Therefore, Eq. (13) should not be used in future modeling efforts. Fig. 3 illustrates this discrepancy.

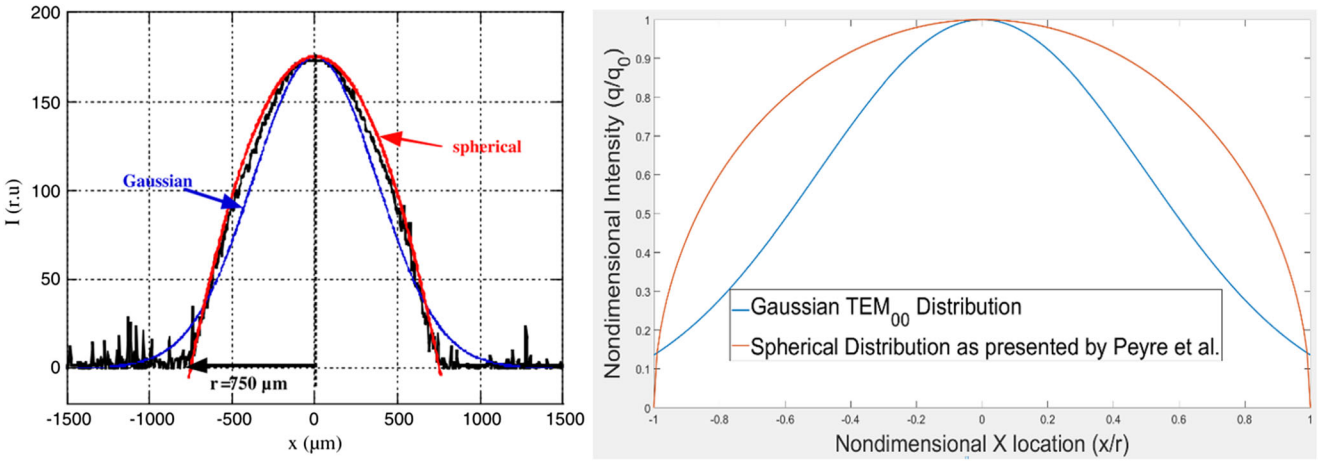

Fig. 3 Comparison between experimental laser beam distribution, spherical, and Gaussian approximations as presented by Peyre et al. [36] (left); comparison of Gaussian distribution (Eq. (1)) to circular distribution (Eq. (13)).

3.2 Three-dimensional models

3.2.1 Gaussian ellipsoid

The physical and geometrical characteristics of the model can be examined to confirm its validity. This procedure is rather straightforward in the case of the ellipsoidal model, since a full mathematical derivation was provided by Goldak et al. [38, 65].

The intensity equation is first integrated over its entire domain in the X, Y, and Z axes to confirm that the model upholds the law of energy conservation. For convenience, a z axis that travels along with the heat source is considered, as opposed to the stationary ξ axis. This integral is given by:

$$Q_{Model} = \int_0^c\int_{-b}^b\int_{-a}^a q(x,y,z)\,dx\,dy\,dz = \frac{6\sqrt{3}Q_{Actual}}{abc\pi\sqrt{\pi}}\int_0^c\int_{-b}^b\int_{-a}^a e^{-3x^2/a^2}e^{-3y^2/b^2}e^{-3z^2/c^2}dx\,dy\,dz \tag{30}$$

where Q_{Model} is the theoretical value of total heat energy emitted by the heat source, obtained by integrating the intensity function over its entire volumetric domain. Q_{Actual}, the actual value of total heat emitted by the source, is the value used to calculate the intensity distribution in the first place. By comparing the values of Q_{Model} and Q_{Actual}, one can obtain an estimate of the physical validity and consistency of the heat source model. Evaluating these integral yields:

$$Q_{Model} = \frac{6\sqrt{3}Q_{Actual}}{abc\pi\sqrt{\pi}}\int_0^c\int_{-b}^b\int_{-a}^a e^{-3x^2/a^2}e^{-3y^2/b^2}e^{-3z^2/c^2}\,dx\,dy\,dz$$
$$= \frac{6Q_{Actual}}{bc\pi}\mathrm{erf}\left(\sqrt{3}\right)\int_0^c\int_{-b}^b e^{-\frac{3y^2}{b^2}}e^{-\frac{3z^2}{c^2}}\,dy\,dz = \frac{6Q_{Actual}}{c\sqrt{3\pi}}\mathrm{erf}^2\sqrt{3}\int_0^c e^{-\frac{3z^2}{c^2}}\,dz$$
$$\therefore Q_{Model} = Q_{Actual}{}^{*}\mathrm{erf}^3\sqrt{3} \tag{31}$$

Therefore, by integrating the intensity function over its domain, the value of Q_{Model} is found to be $0.9577(Q_{\text{Actual}})$. These two values are not perfectly equal due to the assumption that intensity at each edge of the heat-affected zone (HAZ) is equal to 5% of the maximum intensity, which means that only ~95.8% of the heat input is accounted for within the region. Gaussian distributions are inherently asymptotic and thus a decision must be made on what percentage of the total distribution needs to be accounted for.

3.2.2 Gaussian cone

As with the Gaussian ellipsoidal model, this conical model is integrated over its entire domain to test for physical accuracy and consistency. Expressing the model in Cartesian coordinates, the integration is given by:

$$Q_{Model} = \int_0^H\int_{-y_0}^{y_0}\int_{-x_0}^{x_0} q(x,y,z)dx\,dy\,dz \tag{32}$$
$$= \frac{16\,\eta Q_{Actual}}{\pi\left(x_0^2+y_0^2\right)H}\int_0^H\int_{-y_0}^{y_0}\int_{-x_0}^{x_0} e^{-8\left(\frac{x^2+y^2}{x_0^2+y_0^2}\right)}\left(1-\frac{z}{H}\right)dx\,dy\,dz$$
$$= \frac{4\sqrt{2}\eta Q_{Actual}}{\sqrt{\pi\left(x_0^2+y_0^2\right)H}}\mathrm{erf}\left(\frac{2\sqrt{2}x_0}{\sqrt{x_0^2+y_0^2}}\right)\int_0^H\int_{-y_0}^{y_0} e^{-8\left(\frac{y^2}{x_0^2+y_0^2}\right)}\left(1-\frac{z}{H}\right)dy\,dz$$
$$= \frac{2\eta Q_{Actual}}{H}\mathrm{erf}\left(\frac{2\sqrt{2}x_0}{\sqrt{x_0^2+y_0^2}}\right)\mathrm{erf}\left(\frac{2\sqrt{2}y_0}{\sqrt{x_0^2+y_0^2}}\right)\int_0^H\left(1-\frac{z}{H}\right)$$
$$= \eta Q_{Actual}\mathrm{erf}\left(\frac{2\sqrt{2}x_0}{\sqrt{x_0^2+y_0^2}}\right)\mathrm{erf}\left(\frac{2\sqrt{2}y_0}{\sqrt{x_0^2+y_0^2}}\right)$$

In the case of a circular spot size, this integral evaluates to $Q_{Model} \cong 0.991Q_{Actual}$, indicating a strong agreement between the actual and modeled bulk heat input.

For a given penetration depth, substituting $r = 0$ gives the intensity value at the center of the spot, i.e., the maximum intensity at this particular penetration depth.

Substituting $r = r_0$ gives the intensity value at the edge of the spot. The ratio of intensity at the edges to maximum intensity, at a given penetration depth, is equal to $(\exp(-8)/1) = 0.0335\%$. This ratio implies physical consistence; it is low enough that the distribution can be said to effectively decay to zero at the edges. The linear decay of intensity with penetration depth can be seen to decay to zero by simple observation.

3.2.3 Non-Gaussian cone

The intensity distribution is integrated over its domain to investigate how much of the total energy input it accounts for. For ease of understanding and consistent notation, the model is expressed in Cartesian coordinates for this triple integral, using Pythagoras' theorem. This integration yields:

$$
\begin{aligned}
Q_{Model} &= \int_0^H \int_{-y_0}^{y_0} \int_{-x_0}^{x_0} q(x,y,z)\,dx\,dy\,dz \qquad (33)\\
&= \frac{2Q_{Actual}}{\pi\left(x_0^2+y_0^2\right)H} \int_0^H \int_{-y_0}^{y_0} \int_{-x_0}^{x_0} e^{1-\left(\frac{x^2+y^2}{x_0^2+y_0^2}\right)} \left(1-\frac{z}{H}\right) dx\,dy\,dz\\
&= \frac{2Q_{Actual}}{\sqrt{\pi\left(x_0^2+y_0^2\right)}H} \operatorname{erf}\left(\frac{x_0}{\sqrt{x_0^2+y_0^2}}\right) \int_0^H \int_{-y_0}^{y_0} e^{1-\left(\frac{y^2}{x_0^2+y_0^2}\right)} \left(1-\frac{z}{H}\right) dy\,dz\\
&= \frac{2Q_{Actual}}{H} \operatorname{erf}\left(\frac{x_0}{\sqrt{x_0^2+y_0^2}}\right) \operatorname{erf}\left(\frac{y_0}{\sqrt{x_0^2+y_0^2}}\right) \int_0^H \left(1-\frac{z}{H}\right)\\
&= Q_{Actual} \operatorname{erf}\left(\frac{x_0}{\sqrt{x_0^2+y_0^2}}\right) \operatorname{erf}\left(\frac{y_0}{\sqrt{x_0^2+y_0^2}}\right) e^1
\end{aligned}
$$

In the most common case of a circular spot size, where $x_0 = y_0$, this integral evaluates to $Q_{\text{Model}} \cong 1.267 Q_{\text{Actual}}$, indicating that the heat source model overestimates the heat input to the HAZ by over 25%.

By following the previous procedure, the boundary conditions implied by the model can be identified. The intensity boundary condition is thus found to be 36.78% at any given penetration depth. This value seems clearly at odds with the recorded behavior of concentrated heat sources in the literature, as the heat gradient depicted by this model seems largely understated.

Although the exponentially decaying conical distribution represented by this model is geometrically accurate, the model is deemed inadequate due to its considerable overestimation of the total energy transfer and its physically unrealistic boundary conditions.

3.2.4 Other three-dimensional models

The line and elongated ellipsoid models are both based on the Goldak ellipsoidal model, incorporating different averaging methodologies to improve computational efficiency. The physical validity of these models has therefore been discussed previously in Section 3.2.1. Care must be taken when applying these models to follow the guidelines set by Irwin and Michaleris and ensure that a reasonable trade-off between computational efficiency and accuracy is being obtained.

An indefinite integral of the three-dimensional TEM_{00} model cannot be obtained, and therefore its adherence to energy conservation could not be validated.

For the logarithmic decay model, at a constant penetration depth of $z = H$, the antiderivative of the model is found and yields the following result:

$$Q_{Model} = Q_{Actual} * erf^2\left(\sqrt{3c_s}r\right) \qquad (34)$$

which leads to the conclusion that the accuracy of this model is dependent on correct selection of the shape factor. Yu et al. used a value of $c_s = \frac{3}{r^2}$ in their study, which leads to nearly 100% energy conservation. Evaluating the intensity at the edge and center of the spot at this depth and shape factor, $I_{bc} = 1.11\%$. The model performs well in terms of the metrics defined in this study; however, this does not address the difficulty in using the model due to the discontinuities it introduces due to the logarithmic term in the denominator of the exponential function.

3.3 Summary

To sum up the review and analysis presented in this paper, This analysis has shown that, while most heat source models used in the additive manufacturing literature abide by conservation of energy principles represent realistic boundary conditions, some of the models do not. In surface models, using a laser distribution factor of 1 in the TEM00 model does not only influence the radial decay profile, but it also considerably underestimates the incident irradiation which is problematic. The circular distribution is divergent and thus not presumed invalid. With volumetric models, the non-Gaussian cone vastly overestimates incident irradiance, and the 3D TEM00 model is not integrable and thus can only be tested numerically; it also yields and *I*_bc value that is dependent on r, and therefore the radius of the spot size will determine the radial decay profile.

Table 1 shows all heat source models discussed herein as well as key details about each of them.

This analysis has shown that, while most heat source models used in the additive manufacturing literature abide by conservation of energy principles represent realistic boundary conditions, some of the models do not. In surface models, using a laser distribution factor of 1 in the TEM_{00} model does not only influence the radial decay profile, but it also considerably underestimates the incident irradiation which is problematic. The circular distribution is divergent and thus not presumed

Table 1 Summary of heat source models used in the AM literature

Model type	Model name	First use in AM literature	Energy conservation*	Boundary condition I_{bc}**
Two-dimensional (surface)	TEM_{00}	Hu and Kovacevic [4]	91.1%	13.5%
	Modified TEM_{00}	Manvatkar et al. [23]	97.2%	5.0%
	$TEM_{00} + TEM_{01}$	Kovalev et al. [32]	95.8***	$\frac{a_{00}+2a_{01}}{a_{00}} e^{-2}$ ***
	Circular Gaussian	Peyre et al. [36]	Undefined	0%
Three-dimensional (volumetric)	Gaussian Ellipsoid	Lundbäck and Lindgren [66]	95.8%	5.0%
	Gaussian Cone	Shen and Chou [50]	99.1%	0.0335%
	Non-Gaussian Cone	Wang and Felicelli [54]	126.7%	36.78%
	Line/ Elongated Ellipsoid	Irwin and Michaleris [58]	95.8%	5.0%
	3D TEM_{00}	Vasquez et al. [59]	Undefined	$e^{\frac{-2\sqrt{2}}{r}}$
	Logarithmic Decay	Yu et al. [62]	100.0 %	1.11%

*Percentage of incident laser irradiance accounted for by the heat source model

**Ratio of laser intensity at the edge of the laser spot to laser intensity at the center of the spot, indicating the gradient of energy decay. Evaluated at a constant penetration depth for volumetric models

***Assuming the focal plane is positioned at the deposition site

invalid. With volumetric models, the non-Gaussian cone vastly overestimates incident irradiance, and the 3D TEM_{00} model is not integrable and thus can only be tested numerically; it also yields and I_{bc} value that is dependent on r, and therefore the radius of the spot size will determine the radial decay profile.

4 Discussion and conclusions

This paper has presented an overview of heat source models used to date in the thermal modeling of additive manufacturing processes. The models were presented in the context of their original work, and then their validity was investigated. Two non-dimensional parameters were defined to carry out the investigation:

- The ratio of total irradiation accounted for by each model, Q_{Model} to incident irradiation, Q_{Actual}, was calculated. This provides insight on whether or not a model abides by the first law of thermodynamics.
- The ratio of minimum intensity (at the edge of the spot) to maximum intensity (at the center of the spot) was calculated. This provides insight into the radial decay profile of the model.

First, two-dimensional surface models were presented and discussed. These models portray a surface distribution of laser energy on the deposition surface, which is accurate to how laser energy dissipates on a solid metal surface. However, when using these models other accommodations must be made to account for the various physical phenomena occurring at the deposition site: Changes in absorptivity of the metal, molten pool stirring, and convection due to the Marangoni effect are some of these phenomena. The findings in this section can be summarized as follows:

- The classic TEM_{00} equation is a reliable, easy-to-use model that provides a reasonable estimation of the heat distribution profile. Some authors opt to use this model with a different laser distribution factor: a factor of 3 seems to provide a more accurate representation of the heat distribution according to the metrics considered in this study, but further investigation is required to ensure that its decay profile remains reasonably close to experimental findings. Using a laser distribution factor of 1 in the TEM_{00} model causes considerable violation of the first law of thermodynamics and yields unreasonable boundary conditions. It is therefore not recommended.
- The combination TEM_{00}/TEM_{01} model upholds the first law of thermodynamics and appears to function as intended. This model is useful when laser irradiance cannot be retained at the TEM_{00} mode, although attempts must be made to do so as the TEM_{00} mode provides the most efficient transfer of energy for the purposes of additive manufacturing.
- The circular distribution model is divergent and thus is deemed invalid.

A discussion of three-dimensional volumetric heat source models was then presented. These models assume a volumetric dissipation of laser energy, with an axial component penetrating into the surface of the deposition site. These models estimate the entire heat dissipation process in the substrate along with all related phenomena and have been used repeatedly by researchers to obtain accurate results while avoiding the complexity of multi-scale, multi-physics modeling. These models require extensive tuning using experimental data,

where values of equation constants are typically unique to specific experimental conditions and cannot be extended to other situations.

- Goldak's ellipsoidal model remains a straightforward and accurate model that applicable to a variety of cases.
- The Gaussian cone model presented by Rogeon et al. also performs well, meeting all the required physical and mathematical restrictions. This model's linearly decaying penetration is claimed to be better suited for high-energy applications.
- The non-Gaussian cone proposed by Tsirkas et al. imposes inaccurate boundary conditions and overestimates the total incident irradiance and is thus deemed an inadequate model.
- The line model and the elongated ellipsoidal model, both based on Goldak's ellipsoidal model, attempt to maintain the accuracy of that model while allowing for fewer time steps, requiring less computational resources. Both models appear to function well and can be used effectively in some applications, pending further investigation. Care must be taken to ensure that the parameters used do not result in averaging errors or a discontinuous thermal field. These tools must be used carefully with a thorough understanding of the underlying mathematics.
- The origins of the three-dimensional TEM_{00} model are unclear. It is also non-integrable and thus its adherence to the first law of thermodynamics could not be established. Its boundary condition is dependent on the spot radius, which indicates that it might only be suitable for specific spot sizes. Further study is needed to confirm the validity of this model.
- The logarithmic decay model is discontinuous at a penetration depth of zero, which renders it difficult to use numerically. It does, however, abide by the first law of thermodynamics and utilize appropriate boundary conditions.

Acknowledgements The authors acknowledge financial support from the National Science and Engineering Research Council (NSERC) and Ontario Centres of Excellence (OCE).

References

1. Arrizubieta J, Tabernero I, Exequiel Ruiz J, Lamikiz A, Martinez S, Ukar E (2014) Continuous coaxial nozzle design for LMD based on numerical simulation. 56:429–438
2. Thompson SM, Bian L, Shamsaei N, Yadollahi A (2015) An overview of direct laser deposition for additive manufacturing; part I: transport phenomena, modeling and diagnostics. Addit Manuf 8:36–62
3. De Freitas Teixeira PR, De Araújo DB, Da Cunha LAB (2014) Study of the Gaussian distribution heat source model applied to numerical thermal simulations of tig welding processes. Cienc y Eng Sci Eng J 23(1):115–122
4. Hu D, Kovacevic R (2003) Modelling and measuring the thermal behaviour of the molten pool in closed-loop controlled laser-based additive manufacturing. Proc Inst Mech Eng Part B J Eng Manuf 217(4):441–452
5. Cline HE, Anthony TR (1977) Heat treating and melting material with a scanning laser or electron beam. J Appl Phys 48(9):3895–3900
6. CVI Melles Griot (2009) Gaussian Beam Optics. Gaussian Beam Opt 2(1)
7. Han L, Phatak KM, Liou FW (2004) Modeling of laser cladding with powder injection. Metall Mater Trans B Process Metall Mater Process Sci 35(6):1139–1150
8. Frenk A, Vandyoussefi M, Wagniere J-D, Zryd A, Kurz W (1997) Analysis of the laser-cladding process for stellite on steel. Metall Mater Trans B Process Metall Mater Process Sci 28B(June):501–508
9. Qi H, Mazumder J, Ki H (2006) Numerical simulation of heat transfer and fluid flow in coaxial laser cladding process for direct metal deposition. J Appl Phys 100(2)
10. Roberts IA, Wang CJ, Esterlein R, Stanford M, Mynors DJ (2009) A three-dimensional finite element analysis of the temperature field during laser melting of metal powders in additive layer manufacturing. Int J Mach Tools Manuf 49(12–13):916–923
11. Hitz CB, Ewing J, Hecht J (2012) Introduction to Laser Technology
12. Fischer P, Locher M, Romano V, Weber HP, Kolossov S, Glardon R (2004) Temperature measurements during selective laser sintering of titanium powder. Int J Mach Tools Manuf 44(12–13):1293–1296
13. Lavery NP, Brown SGR, Sienz J, Cherry J (2014) A review of computational modelling of additive layer manufacturing – multi-scale and multi-physics. Sustain Des Manuf 1(1):651–673
14. Zeng K, Pal D, Stucker BE (2012) A review of thermal analysis methods in laser sintering and selective laser melting. Proc Solid Free Fabr Symp 796–814
15. Alimardani M, Toyserkani E, Huissoon JP, Paul CP (2009) On the delamination and crack formation in a thin wall fabricated using laser solid freeform fabrication process: an experimental-numerical investigation. Opt Lasers Eng 47(11):1160–1168
16. Picasso M, Rappaz M (1994) A simple but realistic model for laser cladding. Metall Mater Trans B Process Metall Mater Process Sci 25(2):281–291
17. Steen WM, Mazumder J (2010) Laser material processing. Springer, New York
18. Kovalev OB, Kovaleva IO, Smurov IY (2017) Numerical investigation of gas-disperse jet flows created by coaxial nozzles during the laser direct material deposition. J Mater Process Technol 249(June):118–127
19. Toyserkani E (1970) Laser Cladding. CRC Press, Boca Raton
20. Foteinopoulos P, Papacharalampopoulos A, Stavropoulos P (2018) On thermal modeling of additive manufacturing processes. CIRP J Manuf Sci Technol 20:66–83
21. Cernuschi F, Ahmaniemi S, Vuoristo P, Mäntylä T (2004) Modelling of thermal conductivity of porous materials: application to thick thermal barrier coatings. *J Eur Ceram Soc* 24(9):2657–2667
22. German RM, Park SJ (2008) Handbook of mathematical relations in particulate materials processing: ceramics, powder metals, cermets, carbides, hard materials, and minerals. John Wiley & Sons, Inc.
23. Manvatkar VD, Gokhale AA, Jagan Reddy G, Venkataramana A, De A (2011) Estimation of melt pool dimensions, thermal cycle, and hardness distribution in the laser-engineered net shaping process of austenitic stainless steel. Metall Mater Trans A Phys Metall Mater Sci 42(13):4080–4087
24. Manvatkar V, De A, Debroy T (2014) Heat transfer and material flow during laser assisted multi-layer additive manufacturing. J Appl Phys 116(12)
25. Manvatkar V, De A, DebRoy T (2015) Spatial variation of melt pool geometry, peak temperature and solidification parameters

during laser assisted additive manufacturing process. Mater Sci Technol 31(8):924–930
26. Mukherjee T, Zhang W, DebRoy T (2017) An improved prediction of residual stresses and distortion in additive manufacturing. Comput Mater Sci 126:360–372
27. Huang YL, Liang GY, Su JY, Li JG (2005) Interaction between laser beam and powder stream in the process of laser cladding with powder feeding. Model Simul Mater Sci Eng 13(1):47–56
28. Born M, Wolf E, Bhatia AB (1980) Principles of optics : electromagnetic theory of propagation, interference and diffraction of light, 6th edn. Pergamon Press, Oxford
29. Kerker M (1969) The Scattering of Light; And Other Electromagnetic Radiation. Academic Press, New York
30. Jones AR (1983) Calculation of the ratios of complex Riccati-Bessel functions for Mie scattering. J Phys D Appl Phys 16(3)
31. Jia X (2016) Calculation of auxiliary functions related to Riccati–Bessel functions in Mie scattering. J Mod Opt 63(21):2348–2355
32. Kovalev OB, Bedenko DV, Zaitsev AV (2018) Development and application of laser cladding modeling technique: from coaxial powder feeding to surface deposition and bead formation. Appl Math Model 57:339–359
33. Kovalev OB, Zaitsev AV, Novichenko D, Smurov I (2011) Theoretical and experimental investigation of gas flows, powder transport and heating in coaxial laser direct metal deposition (DMD) process. J Therm Spray Technol 20(3):465–478
34. Bedenko DV, Kovalev OB, Smurov I, Zaitsev AV (2016) Numerical simulation of transport phenomena, formation the bead and thermal behavior in application to industrial DMD technology. Int J Heat Mass Transf 95:902–912
35. Novichenko D, Marants A, Thivillon L, Bertrand P, Smurov I (2011) Metal matrix composite material by direct metal deposition. Phys Procedia 12(PART 1):296–302
36. Peyre P, Aubry P, Fabbro R, Neveu R, Longuet A (2008) Analytical and numerical modelling of the direct metal deposition laser process. J Phys D Appl Phys 41(2)
37. Zhao X, Iyer A, Promoppatum P, Yao SC (2017) Numerical modeling of the thermal behavior and residual stress in the direct metal laser sintering process of titanium alloy products. Addit Manuf 14: 126–136
38. Goldak J, Chakravarti A, Bibby M (1984) A new finite element model for welding heat sources. Metall Trans B 15(2):299–305
39. Paley Z, Hibbert PD (1975) Computation of temperatures in actual weld designs. Weld J 54(11):385–392
40. Christensen N, Davies LDV, Gjermundsen K (1965) No Title. Br Weld J 12:54–75
41. Chong LM 1982"Predicting weld hardness," Carleton University
42. Krutz GW, Segerlind LJ (1978) Finited element analysis of welded structures. Weld J Res Suppl 57:211 s–216 s
43. Pavelic V, Tanbakuchi R, Uyehara OA, Myers PS (1969) Experimental and computed temperature histories in gas tungsten arc welding of thin plates. Weld J Res Suppl 48:295–305
44. Michaleris P (2014) Modeling metal deposition in heat transfer analyses of additive manufacturing processes. Finite Elem Anal Des 86:51–60
45. Heigel JC, Michaleris P, Reutzel EW (2015) Thermo-mechanical model development and validation of directed energy deposition additive manufacturing of Ti-6Al-4V. Addit Manuf 5:9–19
46. Yang Q, Zhang P, Cheng L, Min Z, Chyu M, TO AC (2016) Finite element modeling and validation of thermomechanical behavior of Ti-6Al-4V in directed energy deposition additive manufacturing. Addit Manuf 12:169–177
47. Denlinger ER, Michaleris P (2016) Effect of stress relaxation on distortion in additive manufacturing process modeling. Addit Manuf 12:51–59
48. Rogeon Ph, Couedel D, Carron D, et al. (2001) Numerical simulation of electron beam welding of metals: sensitivity study of a predictive model. In: Cerjak H, Bhadeshia H K D H, eds. Mathematical Modelling of Weld Phenomena. Graz: The Institute of Materials, Minerals and Mining, 5:913–943
49. Rouquette S, Guo J, Le Masson P (2007) Estimation of the parameters of a Gaussian heat source by the Levenberg-Marquardt method: application to the electron beam welding. Int J Therm Sci 46(2): 128–138
50. Shen N, Chou K (2012) Thermal modeling of electron beam sdditive manufacturing process: powder sintering effects. In: ASME 2012 International Manufacturing Science and Engineering Conference. p 287
51. Romano J, Ladani L, Sadowski M (2015) Thermal modeling of laser based additive manufacturing processes within common materials. Procedia Manuf 1:238–250
52. Romano J, Ladani L, Sadowski M (2016) Laser additive melting and solidification of Inconel 718: finite element simulation and experiment. Jom 68(3):967–977
53. Tsirkas SA, Papanikos P, Kermanidis T (2003) Numerical simulation of the laser welding process in butt-joint specimens. J Mater Process Technol 134(1):59–69
54. Wang L, Felicelli S (2007) Process modeling in laser deposition of multilayer SS410 steel. J Manuf Sci Eng 129(6):1028
55. Wang L, Felicelli S, Gooroochurn Y, Wang PT, Horstemeyer MF (2008) Optimization of the LENS® process for steady molten pool size. Mater Sci Eng A 474(1–2):148–156
56. Hofmeister W, Wert M, Smugeresky J, Philliber JA, Griffith M (1999) Investigating solidification with the laser-engineered net shaping (LENSTM) process. Miner Met Mater Soc 51(7)
57. Piekarska W, Kubiak M (2012) Theoretical investigations into heat transfer in laser-welded steel sheets. J Therm Anal Calorim 110(1): 159–166
58. Irwin J, Michaleris P (2016) A line heat input model for additive manufacturing. J Manuf Sci Eng 138(11):111004
59. Vásquez F, Ramos-Grez JA, Walczak M (2012) Multiphysics simulation of laser-material interaction during laser powder depositon. Int J Adv Manuf Technol 59(9–12):1037–1045
60. Lalas C, Tsirbas K, Salonitis K, Chryssolouris G (2007) An analytical model of the laser clad geometry. Int J Adv Manuf Technol 32(1–2):34–41
61. Sankaranarayanan S, Kar A (1999) Nonlinear effects of laser-plasma interaction on melt-surface temperature. J Phys D Appl Phys 32(7):777–784
62. Yu G, Gu D, Dai D, Xia M, Ma C, Chang K (2016) Influence of processing parameters on laser penetration depth and melting/re-melting densification during selective laser melting of aluminum alloy. Appl Phys A Mater Sci Process 122(10):1–12
63. Bag S, Trivedi A, De A (2009) Development of a finite element based heat transfer model for conduction mode laser spot welding process using an adaptive volumetric heat source. Int J Therm Sci 48(10):1923–1931
64. Sargent M, Scully MO, Lamb WE (2018) Laser physics
65. Goldak JA, Akhlaghi M (2005) Therm Anal Welds
66. Lundbäck A, Lindgren LE (2011) Modelling of metal deposition. Finite Elem Anal Des 47(10):1169–1177
67. Lindgren LE, Lundbäck A, Fisk M, Pederson R, Anderson J (2016) Simulation of additive manufacturing using coupled constitutive and microstructure models. Addit Manuf 12:144–158